Supporting Information

High Performance Bulk Photovoltaics in Narrow-bandgap Centrosymmetric Ultrathin films

Haoxin Mai, Teng Lu, Qingbo Sun, Robert Elliman, Felipe Kremer, The Duong, Kylie Catchpole, Qian Li, Zhiguo Yi, Terry J. Frankcombe* and Yun Liu**

H. Mai, Dr. T. Lu, Dr. Q. Sun, Prof. Y. Liu, Research School of Chemistry, The Australialian National University, Canberra, ACT 2601, Australia

E-mail: yun.liu@anu.edu.au

Prof. R. Elliman, Research School of Physics and Engineering, The Australialian National University, Canberra, ACT 2601, Australia

Dr. T. J. Frankcombe, School of Physical Environmental and Mathematical Sciences, The University of New South Wales, Canberra, ACT 2601, Australia

Dr. T. Duong, Prof. K. Catchpole, College of Engineering & Computer Science, The University of New South Wales, Canberra, ACT 2601, Australia

Dr. F. Kremer, Centre for Advanced Microscopy, The Australian National University, Canberra, ACT 2601, Australia

Dr Q. Li, Advanced Photon Source, Argonne National Laboratory, Argonne, Illinois 60439, United States

Prof Zhiguo Yi, State Key Laboratory of High Performance Ceramics and Superfine Microstructure, Shanghai Institute of Ceramics, Chinese Academy of Sciences, Shanghai, 200050 China

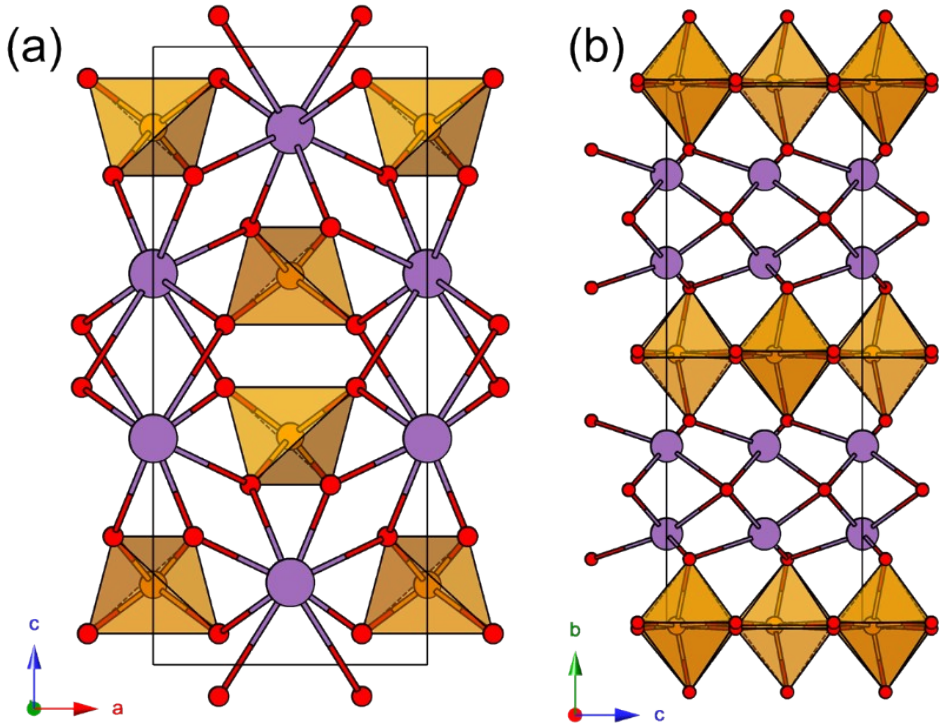

Figure S1 Crystal structures of (a) tetragonal BVO and (b) orthorhombic $Bi_4V_2O_{11}$

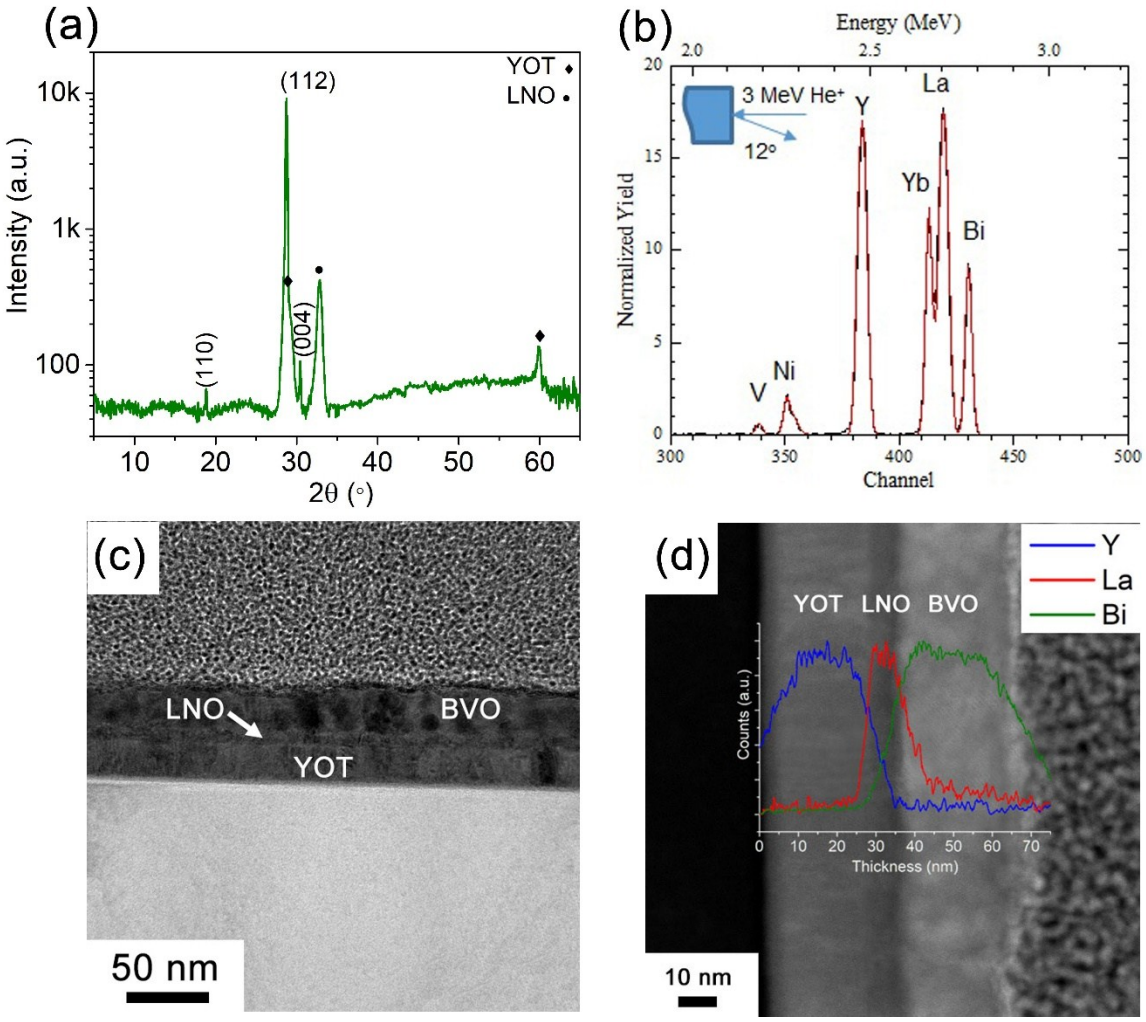

Figure S2 (a) XRD pattern of the 30 nm BVO film deposited on LNO/YOT/Si substrate. (b) He-RBS of the thick BVO film. The Bi/V ratio is calculated as 1.16±0.09. (c) Cross-sectional TEM image of the 30 nm BVO thin film. (d) Cross-sectional dark field TEM image of the 30 nm BVO thin film combining with the corresponding TEM-EDAX line scan. The counts of different elements are normalized respectively.

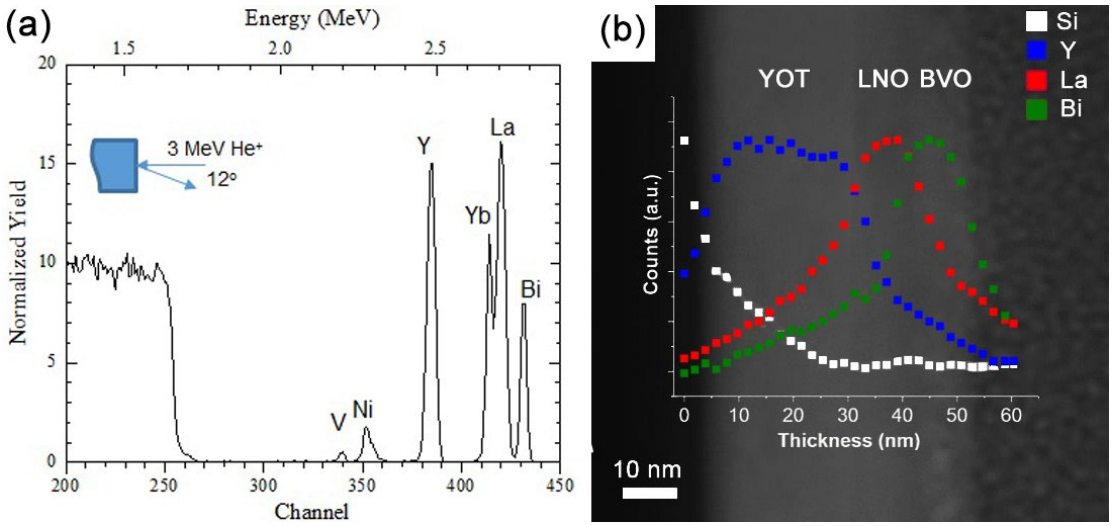

Figure S3 (a) He-RBS of the thin BVO film The Bi/V ratio is calculated as 1.14±0.05. (b) Cross-sectional dark field TEM image of the 10 nm BVO thin film combining with the corresponding TEM-EDAX scans (30 points in a line at the cross-section of the film). The counts of different elements are normalized respectively.

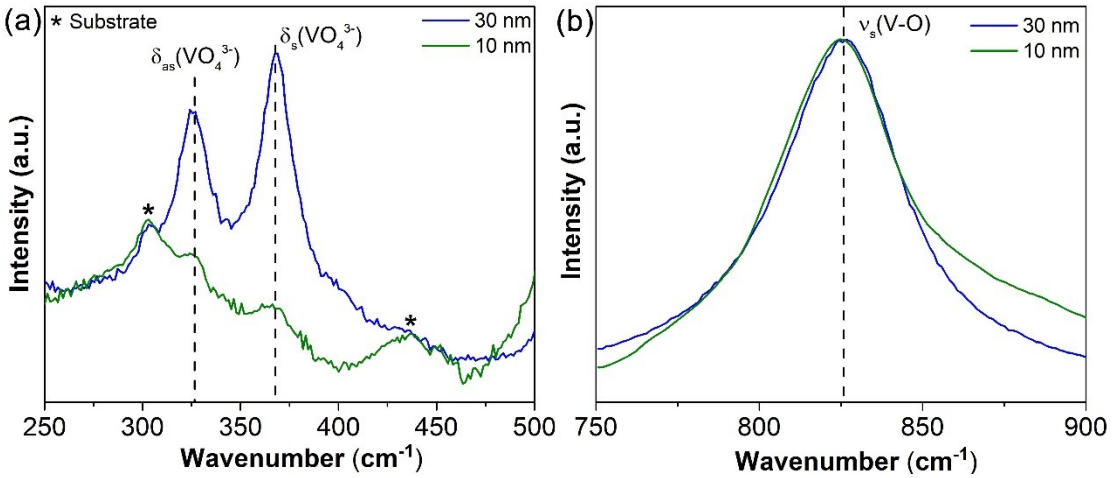

Figure S4 Raman spectra in the (a) 250 – 500 cm^{-1} and (b) 750 – 900 cm^{-1} regions for the 30 nm BVO and the 10 nm BVO deposited on LNO/YOT/Si substrate.

In Figure S4, monoclinic BVO are characterized by the major Raman bands at 828 cm^{-1} attributed to the symmetric V-O stretching (Figure S4b), and the bands at 327 cm^{-1} and 365 cm^{-1} can be assigned to the anti-symmetric and symmetric bending modes of the VO_4 units of the monoclinic BVO (Figure S4a).[1] No bands of other minor phases or compounds are presented. When the thickness of the sample reduces from 30 nm to 10 nm, no significant shift can be observed, and thus we suggest that the structure of BVO remains when reducing thickness.

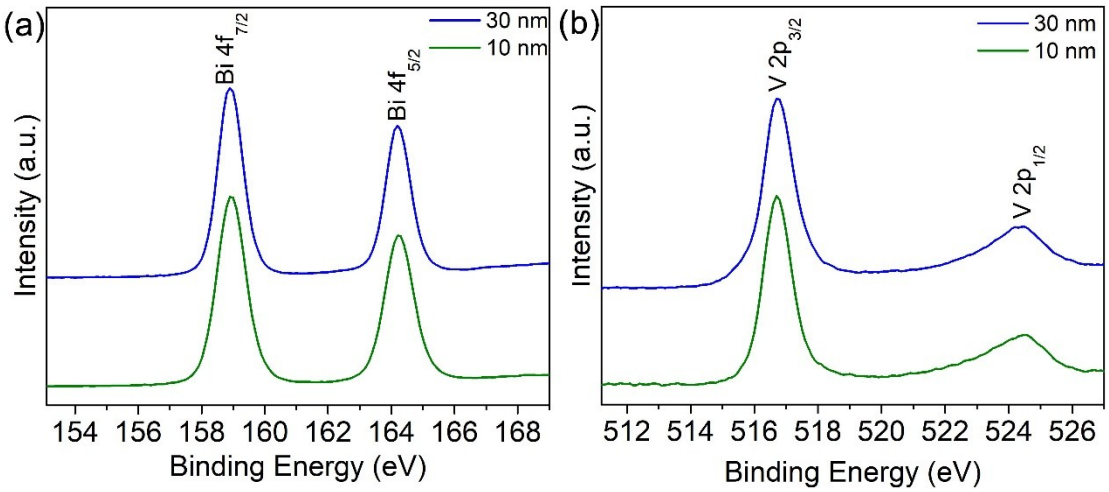

Figure S5 XPS spectra for the BVO films with different thickness: (a) Bi 4f and (b) V 2p. The Bi $4f_{7/2}$ and Bi $4f_{5/2}$ have the binding energies of 159.0 and 164.3 eV, respectively, which can be assigned to the Bi^{3+} in the samples. The binding energies of V $2p_{3/2}$ and V $2p_{1/2}$ are 516.7 eV and 524.6 eV, in agreement with the reported values for the V^{5+} in $BiVO_4$.[2]

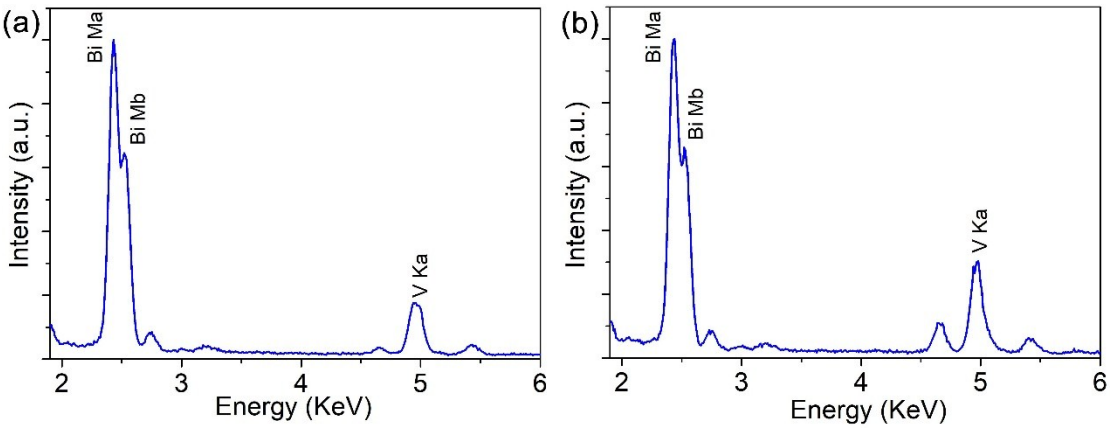

Figure S6 The EDAX analysis of the 30 nm BVO thin film at the region highlighted by (a) red circles and (b) green circle in Figure 2a. The intensity of the peaks are normalized by the intensity of the Bi Ma peak. It is evident from these figures that the ratio of peak intensity of Bi Ma and V Ka in Figure S6a is 5.8, higher than that in Figure S6b (~3), clearly indicating that the region highlighted by red circles have more amounts of Bismuth than the one highlighted by green circle compared with Vanadium.

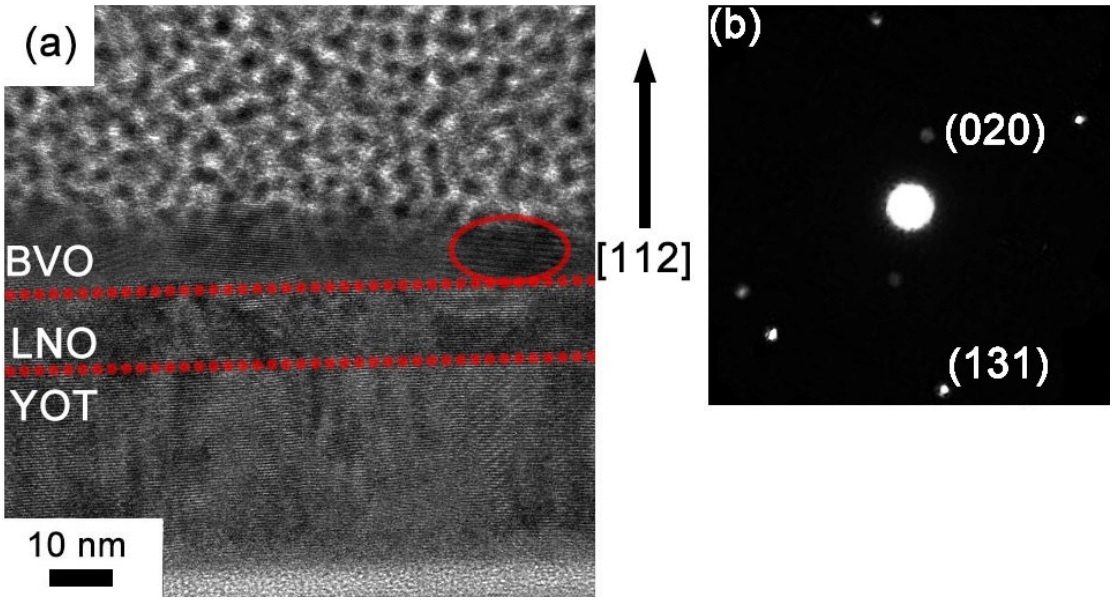

Figure S7 Cross-section HRTEM image of the 10 nm BVO film deposited on LNO-YOT substrate. The interface separating the different layers are indicated with red dot lines. (b) The selected area electron diffraction patterns of the highlighted region.

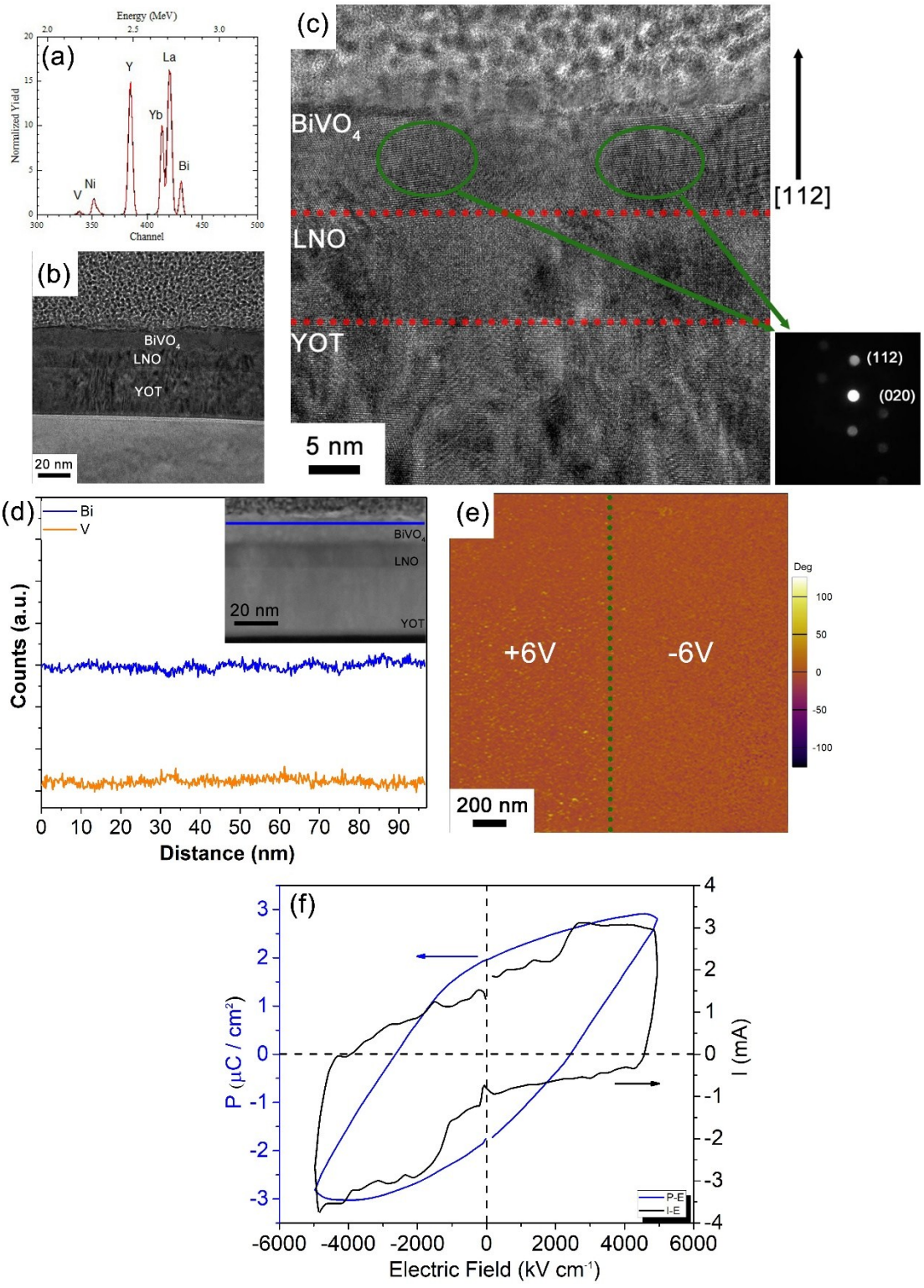

Figure S8 Characterization and ferroelectricity of the 10 nm pure $BiVO_4$ films deposited on LNO/YOT. (a) He-RBS of the thin pure $BiVO_4$ film The Bi/V ratio is calculated as 1.02±0.05. (b) Cross-sectional TEM image of the 10 nm pure $BiVO_4$ film deposited on LNO-YOT substrate. (c) Cross-section HRTEM image of the 10 nm pure $BiVO_4$ film. The interface separating the different layers are indicated with red dot

lines. Inset is the micro-diffraction patterns of highlighted regions in the pure $BiVO_4$ layer. (d) TEM-EDAX line scan in the 10 nm pure $BiVO_4$ layer, inset is the corresponding cross-sectional dark field TEM image (the blue line indicates the scanning line of the EDAX analysis). (e) PFM image of the 10 nm pure $BiVO_4$ films, the written voltage is ±6 V, showing no polar domain observable. (f) *P-E* hysteresis loop and the corresponding *I-E* curve of the pure $BiVO_4$ film. The measurement was performed at the frequency of 2 kHz.

It is widely confirmed that $BiVO_4$ is the intermediate of $Bi_4V_2O_{11}$ in the synthesis of bulk samples when increasing temperature,[3-5] indicating that $Bi_4V_2O_{11}$ is more thermodynamically stable under high temperature than $BiVO_4$. In the case of thin film deposition, the formation of either $BiVO_4$ or $Bi_4V_2O_{11}$ is also sensitive to the substrate temperature. E. Alarcon-Llado et al. found that pure $BiVO_4$ could be obtained when the substrate temperature is 460 °C, while tiny amount of $Bi_4V_2O_{11}$ could be observed when the substrate temperature is 500 °C.[6] Therefore, in our study, the substrate temperature is set as 450 °C to obtain the pure $BiVO_4$ films, and 600 °C for the BVO films with $Bi_4V_2O_{11}$ nanoregions.

In the thin film synthesis of BVO, the post-annealing after deposition would mainly affect the crystallinity of the films rather than the phase and composition. This is confirmed by H. Yoon et al., who deposited the BVO films under low temperature then annealed the sample under various temperature.[7] In their study, they concluded that no phase or composition transition would be induced but only higher crystallinity thin films could be obtained when the post-annealing was increased to 600 °C. Therefore, to ensure the high quality of our thin films, and to guarantee that the quality of the 10 nm BVO films and the 10 nm pure $BiVO_4$ films is comparable, the post-annealing temperature of these two samples is set as 600 °C.

The He-RBS indicates that the average ratio of Bi to V of the 10 nm BVO films deposited under 450 °C is ~1.0 (Figure S8a), which is significantly less than that of the films deposited under 600 °C. Figures S8b and S8c show the cross-sectional TEM images of the 10 nm pure $BiVO_4$ films deposited on the LNO/YOT/Si substrate. The thickness of the $BiVO_4$ layer is confirmed to be around 10 nm, and the well-defined $BiVO_4$/LNO and LNO/YOT interfaces as well as the clear lattice fringes indicate the high crystallinity of this structure. The [112] preferential orientation of the $BiVO_4$ layer along the out-of-plane direction of the LNO/YOT layers is confirmed by the d_{112} of the $BiVO_4$ layer (~0.310 nm, Figure S8c) and the micro-diffraction patterns (Figure S8c, inset), which is in line with the reported tetragonal $BiVO_4$ structure ($I4_1/a$, ICSD 62706), while the in-plane orientation of the $BiVO_4$ layer is random. In contrast to the 10 nm BVO films deposited under 600 °C (with PNRs) (Figure 1), we carefully go through the entire sample but no $Bi_4V_2O_{11}$ lattice fringes and diffraction patterns can be found in this sample. In addition, the TEM-EDAX line scan indicates that both the Bi and V distributions are even, and no abrupt increase of the Bi amount is observed (Figure S8d). Considering the results of He-RBS, HRTEM, micro-diffraction and

EDAX, we suggest that the 10 nm $BiVO_4$ films deposited under 450 °C consists only pure $BiVO_4$ and no $Bi_4V_2O_{11}$ exists.

To study the ferroelectricity of the 10 nm pure $BiVO_4$ films, PFM and Polarization-Electric-field (*P-E*) hysteresis loops are employed. Distinct from the 10 nm BVO films deposited under 600 °C, no bipolar written domains are observed (Figure S8e), neither any switchable PFM responses are found when the written voltage is increased to ±10 V (breakdown voltage). The *P-E* hysteresis loop of 10 nm pure $BiVO_4$ films behaves as the leaky dielectric materials with a relatively small induced polarization (~ 3 $\mu C/cm^2$ at 5000 kV cm^{-1}) (Figure S8f), and no clearly identified current peaks are observed compared with the 10 nm BVO films (Figure S10, green line). Both the *P-E* and *I-E* loops indicate that the 10 nm pure $BiVO_4$ films contain no or ignorable switchable polarizations, which means the 10 nm pure $BiVO_4$ films do not have ferroelectric-like features. These results unambiguously show that there is no ferroelectricity in the 10 nm pure $BiVO_4$ films. According to the above characterizations, the 10 nm BVO films deposited under 600 °C and the 10 nm pure $BiVO_4$ films deposited under 450 °C share the identical thickness, crystallinity, out-of-plane orientation and substrates, while the main difference is that the $Bi_4V_2O_{11}$ nano-regions do not exist in the 10 nm pure $BiVO_4$ films. Therefore, it is rational that the $Bi_4V_2O_{11}$ nano-regions play a vital role in the ferroelectricity of the 10 nm BVO films.

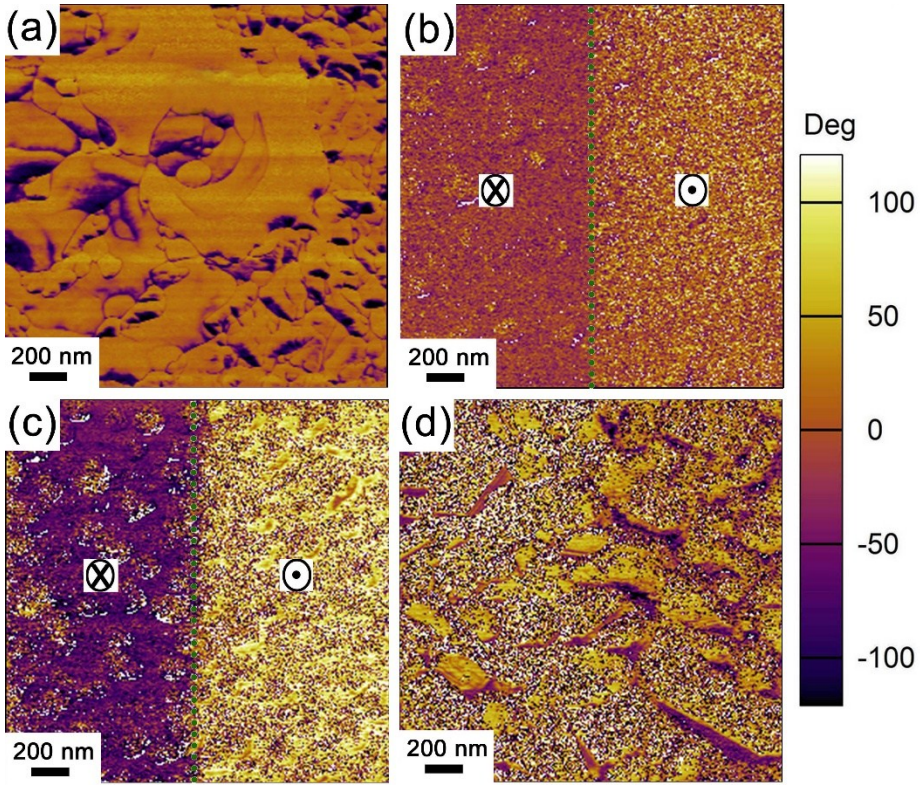

Figure S9 Written domains in BVO films of different thicknesses deposited on Pt substrate. (a) PFM image of the 30 nm BVO film after applying ±18 V written voltage. The written domains of the (b) 15 nm and (c) 10 nm BVO films, the written voltage is ±9 V and ±6 V, respectively. (d) PFM image of the 10 nm pure $BiVO_4$ films deposited under 450 °C, the written voltage is ±6 V.

The deposition of the BVO films on Pt substrates for the PFM images in Figure S9a, S9b and S9c follows the synthesis conditions of the BVO layer (with PNRs) in the MATERIALS AND METHODS section. To synthesize the BVO films on Pt substrate, the laser power density was 2.5 J/cm^2 and the deposition time was 15 min and 5 min for the thick and thin samples, respectively. The oxygen pressure was 1.5×10^{-1} torr, and the substrate temperature was 600 °C. The as-grown thin films were annealed at 600 °C for 30 min under 400 Torr O_2. The deposition of the BVO films on Pt substrate for the PFM image in Figure S9d follows the synthesis conditions of the pure $BiVO_4$ layer (without PNRs) in the MATERIALS AND METHODS section. The laser power density was 2.5 J/cm^2 and the deposition time was 5 min. The oxygen pressure was 1.5×10^{-1} torr, and the substrate temperature was 450 °C. The as-grown thin films were annealed at 600 °C for 30 min under 400 Torr O_2. According to the results from Figure S8, it is expected that pure $BiVO_4$ films will form under this synthesis conditions.

On both the 30 nm BVO films and 10 nm pure $BiVO_4$ films, we attempt the written voltage as high as their breakdown voltage (±30 V for the 30 nm BVO films, and ±10 V for the 10 nm pure $BiVO_4$ films) and no switchable PFM responses can be observed.

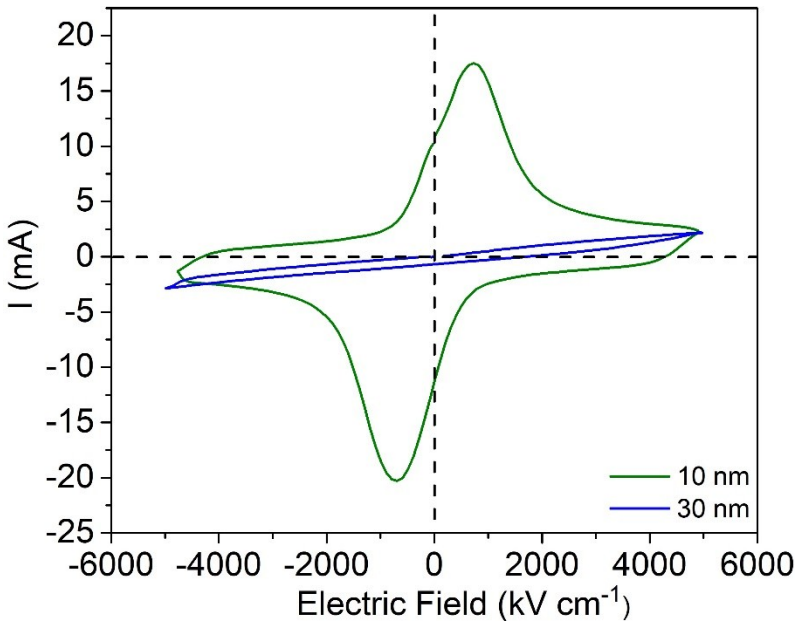

Figure S10 The corresponding *I-E* curves for the *P-E* hysteresis loops of the 10 nm and 30 nm *BVO* thin films shown in Figure 3.

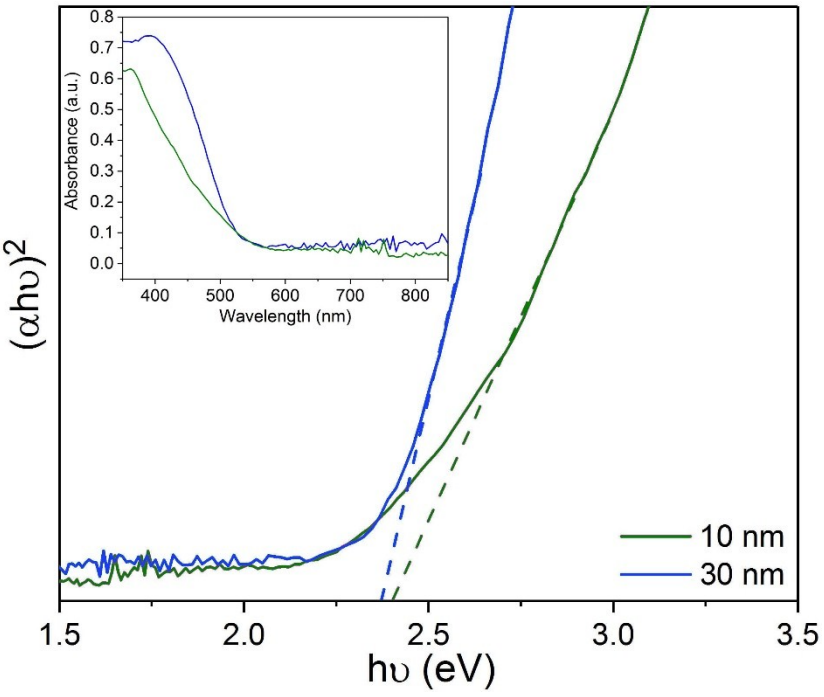

Figure S11 Calculated band gaps of BVO films with the tangent of the linear part as dotted line, inset is the raw UV−vis absorption spectrum.

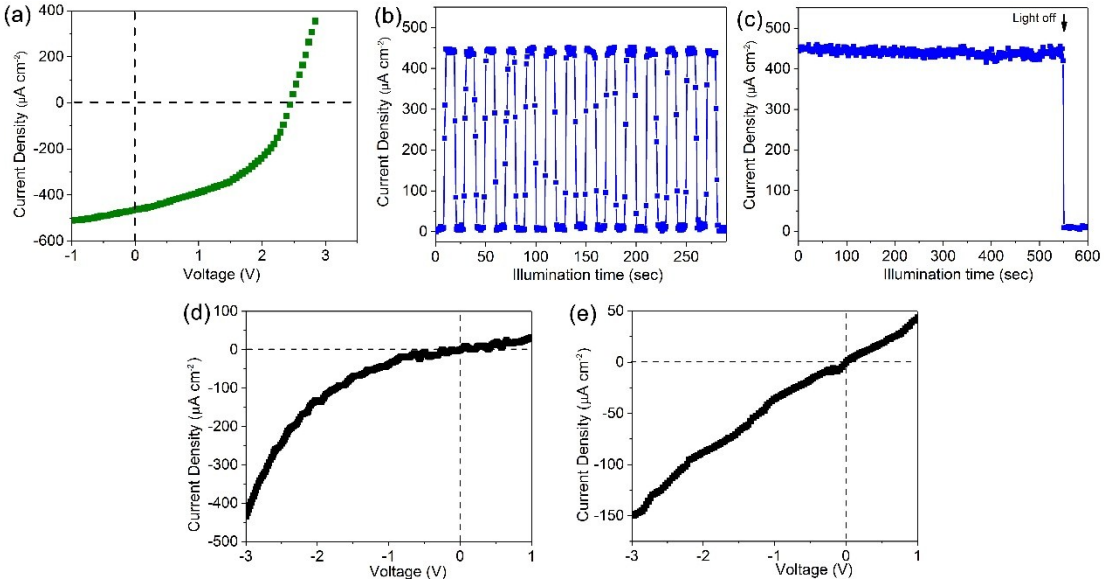

Figure S12 (a) Current−voltage (I−V) characteristics for 10 nm BVO film under AM 1.5G (100 mW cm^{-2}) illumination. Sample was poled by an external electric field towards bottom electrodes. Time dependence of zero bias photocurrent with the illumination (b) ON and OFF and (c) in 600 seconds for the 10 nm BVO films. Current−voltage (I−V) characteristics for 10 nm BVO film (d) in the dark (poled by an external electric field towards top electrodes) and (e) under AM 1.5G (100 mW cm^{-2}) illumination without poling.

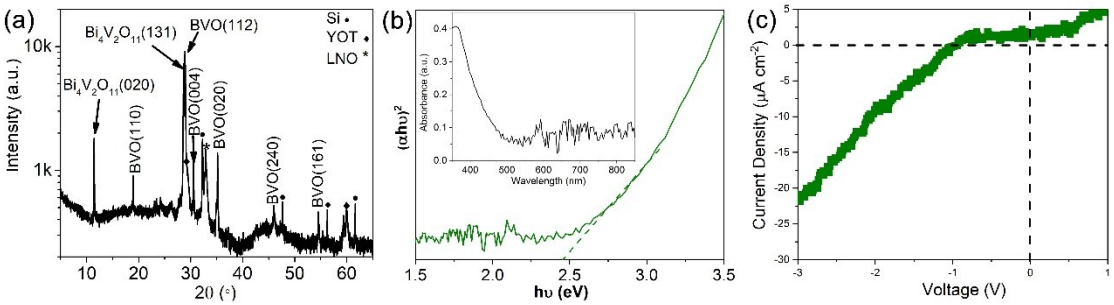

Figure S13 (a) XRD pattern of the thick BVO film. (b) Calculated band gaps of the thin BVO films with the tangent of the linear part as dotted line, inset is the raw UV−vis absorption spectrum. (c) Current−voltage (I−V) characteristics for the thin BVO film under AM 1.5G (100 mW cm^{-2}) illumination. Sample was poled by an external electric field towards top electrodes. All the samples here were deposited on LNO/YOT/Si substrate at 750 °C, the deposition time is 15 min for the thick sample, and 5 min for the thin sample. According to Figure S11, despite the lower bandgap of the $Bi_4V_2O_{11}$ that may absorb more solar spectrum,[8, 9] increasing the amount of $Bi_4V_2O_{11}$ in this system by changing the deposition temperature is found to result in a dramatic drop of the photovoltage and photocurrent, and we assume that this is probably due to the inefficient charge transfer in the $Bi_4V_2O_{11}$ regions and the unfavorable contact between $Bi_4V_2O_{11}/BiVO_4$ under these synthesis conditions.[10]

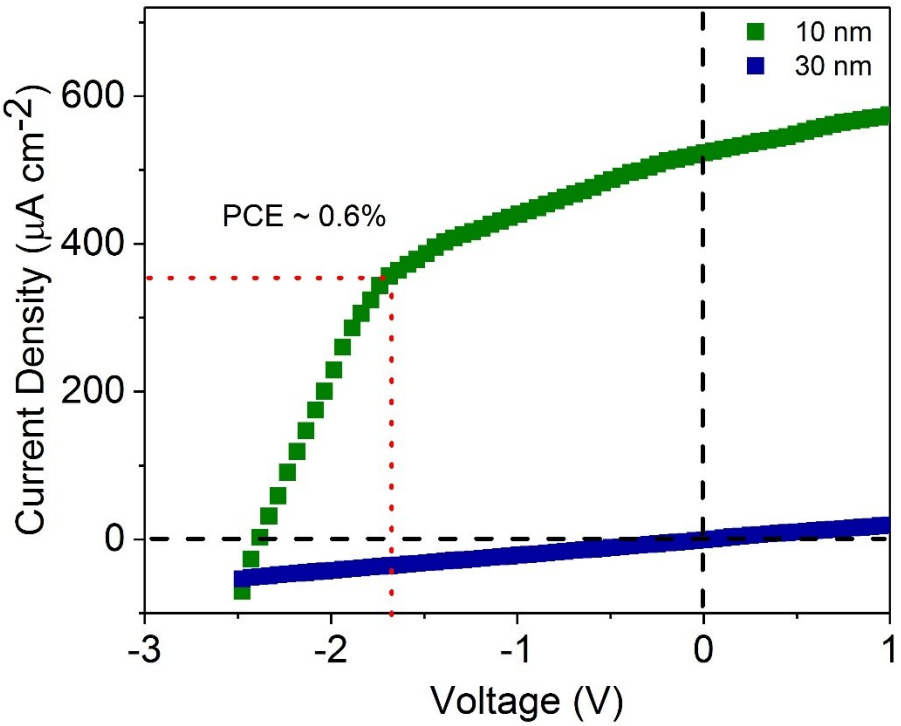

Figure S14 Current−voltage (I−V) characteristics for 10 nm BVO film under AM 1.5G (100 mW cm^{-2}) illumination. Sample was poled by an external electric field towards top electrodes. The PCE of this sample is calculated as 0.6%. The PCE of the bulk counterpart without using our strategy is estimated to be around 0.0006% according to the Figure S6c in the works of Liu et al.,[11] in which the V_{OC} is 41.2 V and the I_{SC} is ~ 1 nA, while the areas of the electrodes are 0.34 × 5.02 mm^2. Since the I-V curve is almost of linearity, the P_{max} will therefore be acquired when V = -20.6 V, which is about 0.0006%, three orders of the magnitude lower than the thin BVO films with the PNRs. We also estimate the PCE according to the other Figures in the works of Liu et al. but find that the maximum PCE is in the case of Figure S6c.[11] Therefore, we suggest that by virtue of our new strategy, the PCE of the narrow-bandgap semiconductor can be improved 1000 times.

References

1. R. L. Frost, D. A. Henry, M. L. Weier and W. Martens, *J Raman Spectrosc*, 2006, **37**, 722-732.
2. Z. Y. Jiang, Y. Y. Liu, T. Jing, B. B. Huang, X. Y. Zhang, X. Y. Qin, Y. Dai and M. H. Whangbo, *J. Phys. Chem. C*, 2016, **120**, 2058-2063.
3. K. Shantha and K. B. R. Varma, *Mat Sci Eng B-Solid*, 1999, **60**, 66-75.
4. K. V. R. Prasad, G. N. Subbanna and K. B. R. Varma, *B Mater Sci*, 1994, **17**, 299-306.
5. J. W. Pell, J. Y. Ying and H. C. Zurloye, *Mater Lett*, 1995, **25**, 157-160.
6. E. Alarcon-Llado, L. Chen, M. Hettick, N. Mashouf, Y. J. Lin, A. Javey and J. W. Ager, *Phys Chem Chem Phys*, 2014, **16**, 1651-1657.
7. H. Yoon, M. G. Mali, J. Y. Choi, M. W. Kim, S. K. Choi, H. Park, S. S. Al-Deyab, M. T. Swihart, A. L. Yarin and S. S. Yoon, *Langmuir*, 2015, **31**, 3727-3737.

8. W. S. dos Santos, M. Rodriguez, A. S. Afonso, J. P. Mesquita, L. L. Nascimento, A. O. T. Patrocinio, A. C. Silva, L. C. A. Oliveira, J. D. Fabris and M. C. Pereira, *Sci Rep-Uk*, 2016, **6**, 31406.
9. Z. Y. Jiang, Y. Y. Liu, M. M. Li, T. Jing, B. B. Huang, X. Y. Zhang, X. Y. Qin and Y. Dai, *Sci Rep-Uk*, 2016, **6**, 22727.
10. C. D. Lv, G. Chen, J. X. Sun, Y. S. Zhou, S. Fan and C. M. Zhang, *Appl Catal B-Environ*, 2015, **179**, 54-60.
11. X. T. Liu, F. Q. Zhang, P. Q. Long, T. Lu, H. R. Zeng, Y. Liu, R. L. Withers, Y. X. Li and Z. G. Yi, *Adv Mater*, 2018, **30**, 1801619.